J Mar Sci Technol (2015) 20:292–308
DOI 10.1007/s00773-014-0283-0

ORIGINAL ARTICLE

Numerical analysis of the interference effects on resistance, sinkage and trim of a fast catamaran

Wei He · Teresa Castiglione · Manivannan Kandasamy · Frederick Stern

Received: 28 April 2014 / Accepted: 24 August 2014 / Published online: 16 September 2014
© JASNAOE 2014

Abstract The purpose of the present paper is the numerical investigation of the interference phenomena between the waves generated by the individual hulls of a catamaran. The study focuses on the effects of both Froude number and demi-hull separation distance on resistance and on sinkage and trim. The numerical simulations are carried out by the URANS solver CFDShip-Iowa V.4 and, to assess the capability for prediction of resistance, sinkage and trim of the URANS code for twin-hull configuration vessels, a verification and validation study is performed for global as well as for local variables. A very good agreement between the numerical results and the experimental data is obtained, and the validation study demonstrates the high level of accuracy of the current predictions, which are used to have a better insight into the interference phenomena. In accordance with the experiments, within $Fr = 0.45$–0.65, the catamaran has a significantly higher resistance coefficient compared to the mono-hull; furthermore, the C_T value increases with decreasing the separation distance between the twin hulls. On the contrary, at Fr lower than 0.45 and at Fr higher than 0.65, the effects of hull spacing on resistance as well as on sinkage and trim can be neglected. The flow field characteristics, wave pattern, wave cuts and pressure distributions are analyzed through the CFD analysis. Finally, the effects of the Reynolds number on resistance are also investigated and results show a small decrease in interference with increasing the Reynolds number.

Keywords URANS · Catamaran · Interference · Verification and validation · CFD · Ship motions · Resistance

W. He and T. Castiglione contributed equally to the present work.

W. He · M. Kandasamy · F. Stern (✉)
IIHR-Hydroscience and Engineering, The University of Iowa, Iowa, IA, USA
e-mail: frederick-stern@uiowa.edu

W. He
School of Naval Architecture, Ocean and Civil Engineering, Shanghai Jiao Tong University, Shanghai, China

T. Castiglione
Department of Mechanical Energy and Management Engineering, University of Calabria, Arcavacata di Rende, Cosenza, Italy

List of symbols

B	Beam of the demi-hull (–)
C_f	Frictional resistance coefficient (–)
C_p	Pressure resistance coefficient (–)
C_r	Residuary resistance coefficient (–)
C_T	Total resistance coefficient (–)
$C_{T,\,cat}$	Catamaran total resistance coefficient (–)
$C_{T,\,mono}$	Mono-hull total resistance coefficient (–)
D	Experimental data value
E	Comparison error
Fr	Froude number $\left(= U/\sqrt{gL_{pp}}\right)$
g	Acceleration of gravity (= 9.81 m/s^2)
h	Water depth (m)
IF	Interference coefficient (–)
k	Turbulent kinetic energy (J/kg)
L_{PP}	Model length (m)
n	Normal direction
p	Order of accuracy, pressure (N/m^2)
p_{th}	Estimated order of accuracy
p_{RE}	Richardson extrapolation order of accuracy
P	Estimated order of accuracy $\left(= \frac{p}{p_{th}}\right)$
r	Grid refinement ratio
R	Ratio between solution changes

Re	Reynolds number ($= \rho UL/\mu$)
R_T	Total resistance (N)
$R_{T,\ cat}$	Catamaran total resistance (N)
$R_{T,\ mono}$	Mono-hull total resistance (N)
S	Separation distance between the hulls [m], wet surface area (m^2)
S_j	Simulation value with grid j
s	Non-dimensional separation distance ($= S/L_{PP}$)
T	Model draft (m)
(U, V, W)	Model velocity components (m/s)
U_D	Data uncertainty
U_{FB}	Facility bias uncertainty
U_G	Grid uncertainty
U_I	Iterative uncertainty
U_{SN}	Numerical simulations uncertainty
U_V	Validation uncertainty
(x, y, z)	Absolute earth-fixed coordinates
(X, Y, Z)	Non-dimensional coordinates
β	Turbulence model constant (–)
δ_{RE}	Numerical error computed by Richardson extrapolation
ε	Turbulence dissipation rate (J/kgs)
ε_{ij}	Difference between solutions i and j
ϕ	Free surface level-set function
λ	Wavelength (m)
ρ	Water density (kg/m^3)
σ	Non-dimensional sinkage
τ	Trim (rad)
ζ_{max}	Highest wave elevation (m)
ω	Specific turbulence dissipation (1/s)

1 Introduction

Multi-hull surface ships are attractive for high-speed uses due to their favorable resistance, transversal stability, and load characteristics in comparison to conventional mono-hulls. Hull types and applications vary considerably: from relatively small foil-assisted high-speed ferries to relatively large SWATH high-speed sealift vessels designed for military transportation. As a consequence, several studies on multi-hull configurations, and in particular on catamarans, have been carried out both experimentally and numerically over the years.

The experimental tests conducted by Insel and Molland [1] and Molland [2], on a high-speed catamaran with symmetric demi-hulls, focus on the effects of hull dimensions and of separation distance, on resistance, sinkage and trim, over a wide range of Froude number values (0.2–1.0). They also developed a numerical model, based on the thin-strip hypothesis, to investigate the catamaran hydrodynamic characteristics. Cheng et al. [3] developed a mathematical theory for the practical design of an asymmetric demi-hull, the *S*-catamaran, whose hull sections were theoretically determined to eliminate or at least substantially reduce wave resistance at supercritical design speeds in shallow water. Further experimental and theoretical investigation of the interference phenomena was also carried out in Millward [4] and Molland et al. [5]. Souto-Igleasias et al. [6] investigated experimentally the influence of the distance between catamaran hulls on wave resistance. They also measured the wave cuts between the two hulls to correlate the shapes of the inner wave cuts with the interference resistance and found the possibility of favorable interference for catamarans.

From a numerical and theoretical point of view, the approaches used for investigation of wave interference effects were commonly based on potential flow theory [7–10]. Bruzzone and Ferrando [11] used a boundary element method in order to study hull separation length effects. Despite the mentioned studies being quite useful to estimate the wave-making resistance and ship motions, issues remain for design improvements, regarding multi-hull interference, reduced wake signatures, deep/shallow water maneuvering, potential flow vs. CFD capability, and optimization. So far, only a few studies have introduced CFD methods for the analysis of multi-hull vessels. Stern et al. [12, 13] have shown interference-induced longitudinal vortices for SWATH. Kandasamy et al. [14] demonstrated the possibility of reduced wake signatures for foil-assisted catamarans. Milanov et al. [15] discussed about the most relevant issues for the improvement of high-speed catamaran deep/shallow watercourse stability design and of system-based method predictions.

Recently, the Delft catamaran [16, 17] has been selected as an international benchmark for research and CFD validation for the Office of Naval Research Naval International Cooperative Opportunities in Science and Technology Program (NICOP) and NATO Advanced Vehicle Technology projects. Several hydrodynamic topics have been assessed about this geometry, by carrying out both experimental tests and numerical studies. They include calm water resistance and seakeeping assessment [18–23], interference effects [24, 25], deep/shallow water maneuvering [15, 26], waterjet propelled optimization [27] and stochastic uncertainty quantification and optimization [28–30]. The numerical studies have been carried out by the use of RANS methods; the use of adaptive grid refinements in Visonneau et al. [26] is worth mentioning.

The present study contributes to this research with the main objective to assess current URANS capability for a high-speed catamaran, including sinkage and trim. In particular, the effects of Froude number (Fr) and demi-hull

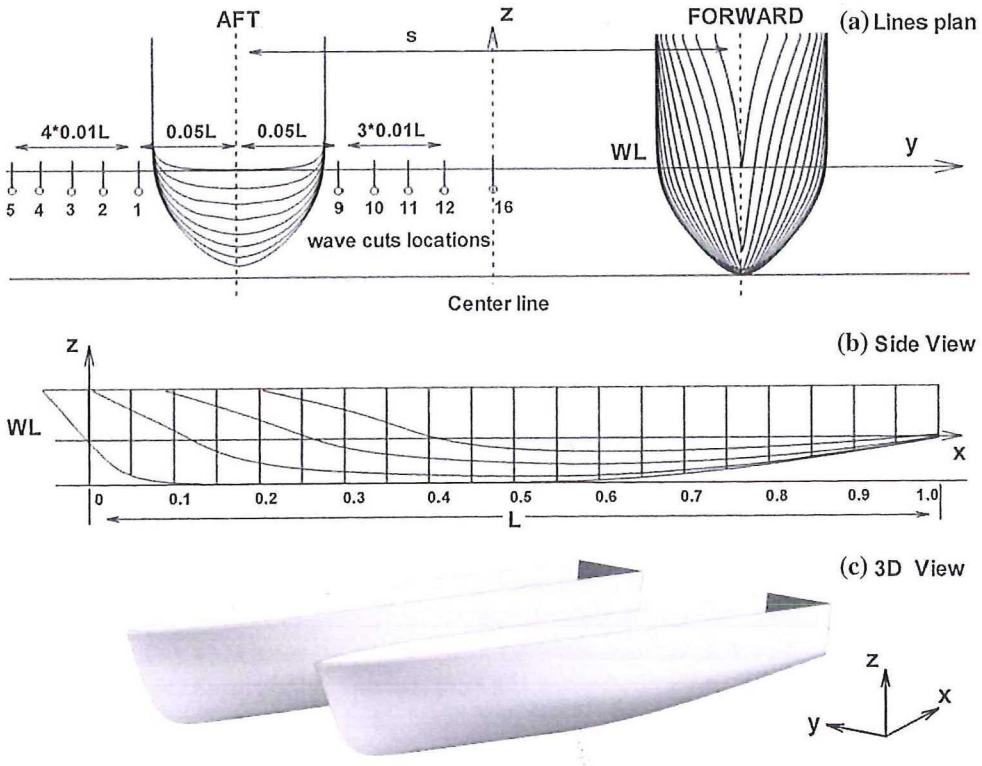

Fig. 1 Lines plan of the Delft catamaran 372. **a** Lines plan **b** Side view **c** 3D View

Table 1 Main particulars of Delft catamaran model

Main particulars	Symbol	Unit	BSHC	TU Delft	INSEAN	CFD
Length between perpendiculars[a]	L_{PP}	m	3.63	3.00	3.00	3.00
Depth of towing tank	h		0.41	0.87	2.17	0.70
Beam overall	B		0.31			
Beam demi-hull	b		0.08			
Distance between center of hulls	s		0.23			
Draft	T		0.05			
Form factor	k		0			
Longitudinal center of gravity	LCG		0.53		0.53	
Vertical center of gravity	KG		0.04		0.06	
Tow point	L_T		[b]		0.53	
	h_T				0.06	
Depth/draft	h/T		8.2	17.3	43.3	14.0
Temperature	C	°C	10.4	20.0	20.1	15.0
Fr range						
C_T, sinkage and trim	Fr		0.17–0.64	0.18–0.75	0.10–0.80	0.30–0.80
Wave cuts				0.3, 0.5, 0.75	0.3, 0.5, 0.75	0.3, 0.5, 0.75
Re (at $Fr = 0.5$)	Re	10^6	9.05	8.13	8.12	7.14
Facility Bias						
C_T	U_{FB}^c		3.11	3.07	4.10	
C_r			3.14	2.63	2.93	
Sinkage			12.77	10.13	4.98	
Trim			3.91	2.80	5.59	

[a] L is dimensional; other length parameters are non-dimensionalized by L

[b] BSHC uses PMM with 2 contact points on the model

[c] U_{FB} is % Max ($D^i_{Avg.}$)

separation distance (s) on resistance, sinkage and trim for the Delft catamaran, are investigated. Simulations are carried out for speed values ranging within $0.3 \leq Fr \leq 0.8$ and include several hull-spacing values varying within $0.17 \leq s \leq 0.30$. The methodology used in this work is as follows: a quantitative verification and validation (V&V) study is performed for $Fr = 0.5$ at the design hull separation distance corresponding to $s = 0.23$, using available benchmark validation data. Once the code is validated, the numerical results are used to have a better insight in the flow field characteristics around the twin hulls; in particular wave pattern, wave cuts in the inner region between hulls and pressure distributions along the hull will be analyzed. Finally, a Reynolds number (Re) study is also included to investigate the effects of viscosity on interference.

2 Overview of experimental data

The main particulars of the Delft catamaran are provided in Fig. 1 and Table 1. For the design separation distance, $s = 0.23$, calm water resistance, sinkage and trim experiments were carried out at three facilities: TU Delft [16], BSHC [31], and INSEAN [24]. The experimental uncertainty (U_D) is provided by INSEAN at $Fr = 0.5$, 0.65 and 0.75. Table 1 also includes the facility bias, U_{FB}, which is estimated by comparing the available data, according to the following approach:

$$U_{FB} = \begin{cases} D^j_{Avg} = \dfrac{1}{M}\sum_{i=1}^{M} D^j_i \\ E^j_i = D^j_i - D^j_{Avg} \\ U_{FB,i} = \dfrac{1}{2}\left[\mathrm{Max}\left(\left|E^j_i\right|\right) - \mathrm{Min}\left(\left|E^j_i\right|\right)\right], \quad j = 1..N \end{cases} \tag{1}$$

where M is the number of facilities where tests are performed, and D^j_i is the observation in ith facility at jth Fr. Facility bias is studied in the Fr range 0.25–0.6 for which the data between facilities overlap.

A comparison of EFD data among the three facilities, at the design separation distance $s = 0.23$, is shown in Fig. 2. It includes total resistance coefficient, C_T, with its friction (C_f) and residuary (C_p) components, and non-dimensional sinkage and trim as functions of the Froude number, Fr. The total resistance coefficient is defined as $C_T = R_T/(0.5\rho U^2 S)$, where R_T is total resistance (N), ρ is density of the water, U is the undisturbed velocity and S is the hull-wetted surface at rest; the non-dimensional sinkage is defined as σ = sinkage/L_{PP}, and the trim angle is expressed as τ, (rad). The measurements have similar trends, but fairly large differences between the facilities occur as indicated by the large U_{FB} values, especially for

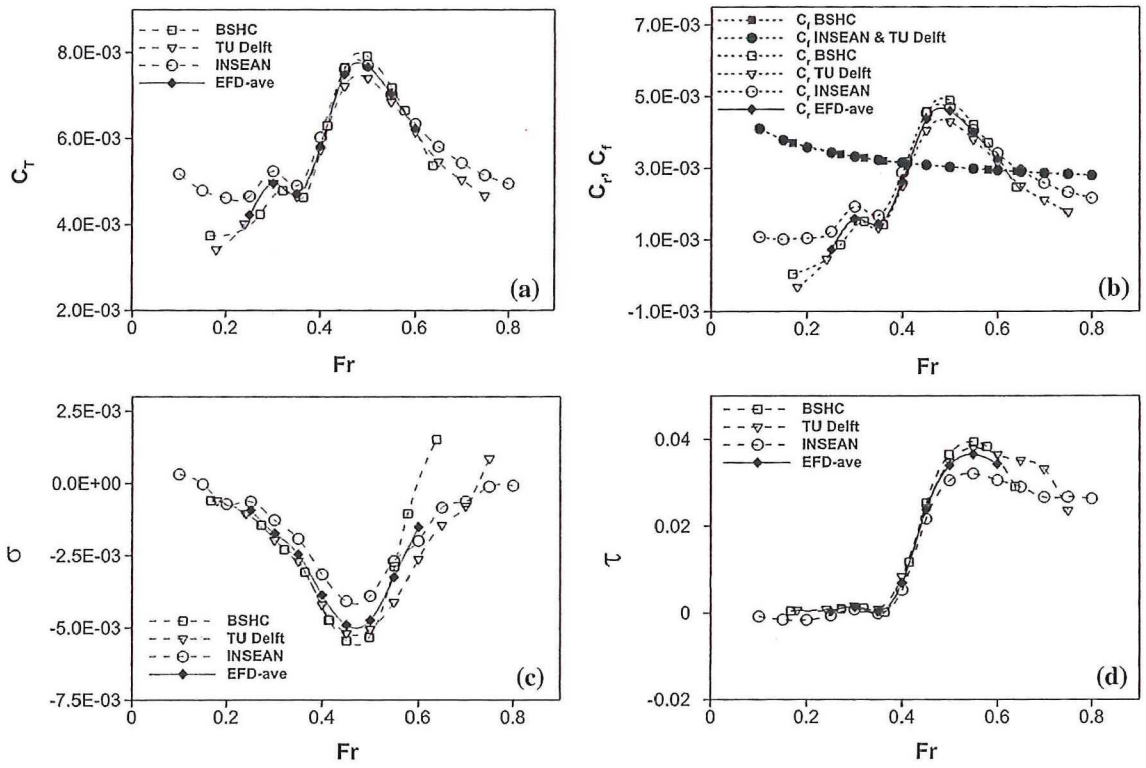

Fig. 2 Comparison of EFD from different facilities at the design separation distance $s = 0.23$. **a** Total resistance coefficient; **b** residuary resistance and friction coefficients; **c** non-dimensional sinkage; **d** non-dimensional trim

sinkage and trim at high Fr. They are due to the different model lengths, depths of the towing tank, temperature and center of gravity position between facilities. Furthermore, TU Delft and INSEAN use conventional resistance single-point mounts, whereas BSHC uses a Planar Motion Mechanism two-point mount. Finally, turbulence simulators are used for INSEAN and TU Delft models but not for BSHC.

INSEAN also provides resistance, sinkage and trim data for the mono-hull and for the catamaran with five separation distances, which vary within 0.17 and 0.30, and for several speed values ($Fr = 0.3$–0.8). The experimental data include the interference coefficient (IF), which is defined as the difference between the total resistance coefficients of the catamaran and the mono-hull, $C_{T,\ cat}$ and $C_{T,\ mono}$ respectively, divided by the mono-hull total resistance coefficient, according to:

$$\mathrm{IF} = \frac{C_{T,cat} - C_{T,mono}}{C_{T,mono}} = \frac{R_{T,cat} - 2R_{T,mono}}{2R_{T,mono}} \tag{2}$$

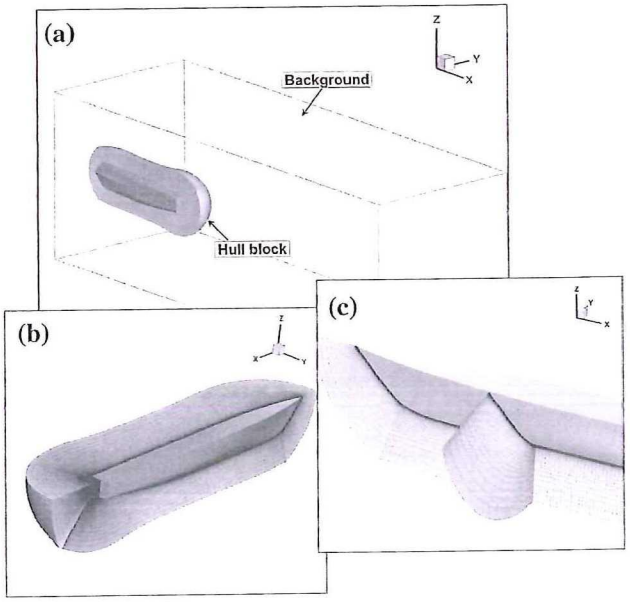

Fig. 3 Particulars of the computation domain

It gives a measure of the interaction between the twin-hull waves systems. It is common, in fact, that for a wide range of ship speed values, the resistance experienced by the twin-hull is higher than twice that of the mono-hull ($R_{T,\ cat} = 2R_{T,\ mono} + R_{IF}$). The additional resistance component is due to the interaction between the waves leaving from each demi-hull, which interact in the inner region. In some cases, negative IF values can occur; the waves systems tend to cancel each other out and cause, therefore, a decrease of wave resistance.

For current URANS simulations, the INSEAN-CNR experimental data [24] will be used for validation purpose. It should be noted that the Reynolds number for CFD simulations is slightly different from the experimental value; this is due to the different water temperature values used between the experiments and the numerical simulations (Table 1). In fact, during the experimental activity it is quite complex to maintain the towing tank water temperature accurate at a prescribed value; consequently, the Reynolds number is usually affected by uncertainty due to changes in viscosity. It is then conventional to use a Reynolds number correction of the experimental data to match Re at 15 °C for consistency, which is the temperature value used for numerical simulations.

3 Computational and analysis method

3.1 Computational method

The code used for the current simulations is CFDShip-Iowa V.4 [32]. It is based on the solution of the unsteady Reynolds Averaged Navier–Stokes equations for the liquid phase of a free surface flow. The free surface is captured using a single-phase level-set method [33], and the turbulence is modeled by a blended $k - \varepsilon/k - \omega$ model [34] without wall functions. Numerical methods include advanced iterative solvers and second- and higher-order finite difference schemes with conservative formulations.

Table 2 Boundary conditions

Description	ϕ	p	k	ω	U	V	W
Inlet ($X = -0.4$)	$\phi = -z$	$\frac{\partial p}{\partial n} = 0$	$\frac{9.0x10^{-3}}{Re}$	9.0	1	0	0
Exit ($X = 3.6$)	$\frac{\partial \phi}{\partial n} = 0$	$\frac{\partial p}{\partial n} = 0$	$\frac{\partial k}{\partial n} = 0$	$\frac{\partial \omega}{\partial n} = 0$	$\frac{\partial^2 U}{\partial n^2} = 0$	$\frac{\partial^2 V}{\partial n^2} = 0$	$\frac{\partial^2 W}{\partial n^2} = 0$
Far-field ($Z = -0.7$)	$\frac{\partial \phi}{\partial n} = 1$	$\frac{\partial p}{\partial n} = 0$	$\frac{\partial k}{\partial n} = 0$	$\frac{\partial \omega}{\partial n} = 0$	1	0	0
Far-field ($Z = 0.7$)	$\frac{\partial \phi}{\partial n} = -1$	–	$\frac{\partial k}{\partial n} = 0$	$\frac{\partial \omega}{\partial n} = 0$	$\frac{\partial U}{\partial n} = 0$	$\frac{\partial V}{\partial n} = 0$	$\frac{\partial W}{\partial n} = 0$
Far-field ($Y = 1.3$)	$\frac{\partial \phi}{\partial n} = 0$	$\frac{\partial p}{\partial n} = 0$	$\frac{\partial k}{\partial n} = 0$	$\frac{\partial \omega}{\partial n} = 0$	$\frac{\partial U}{\partial n} = 0$	$\frac{\partial V}{\partial n} = 0$	$\frac{\partial W}{\partial n} = 0$
Symmetry ($Y = 0$)	$\frac{\partial \phi}{\partial n} = 0$	$\frac{\partial p}{\partial n} = 0$	$\frac{\partial k}{\partial n} = 0$	$\frac{\partial \omega}{\partial n} = 0$	$\frac{\partial U}{\partial n} = 0$	0	$\frac{\partial W}{\partial n} = 0$
No-slip (ship hull)	$\frac{\partial \phi}{\partial n} = 0$	–	0	$\frac{60}{\beta Re \Delta y_1^2}$	0	0	0

Table 3 Grids designed for catamaran studies

Grid	Dimensions			Total	y^+ ($Fr = 0.5$, $Re = 7.1 \times 10^6$)
	Hull in and out	Background	Refinement		
G1R	244 × 93 × 139	436 × 196 × 142	601 × 181 × 181	38.1 M	0.6
G1	244 × 93 × 139	436 × 196 × 142		18.4 M	0.6
G2	172 × 66 × 98	309 × 139 × 101		6.6 M	0.9
G2a	172 × 66 × 98	309 × 139 × 101		6.6 M	0.2
G3	122 × 47 × 70	218 × 98 × 71		2.3 M	1.4
G4	86 × 33 × 49	155 × 70 × 51		0.8 M	2.3

Table 4 Grids and simulation conditions for the different studies

Study	Grid	Simulation conditions		
		Configuration	Fr	Re (10^6)
Verification	G1, G2, G3, G4	$s = 0.23$	0.5	7.14
Interference	G2	Mono-hull, $s = 0.17, 0.23, 0.30$	0.3–0.8	4.29–11.43
Refinement	G1, G1R	$s = 0.17$	0.5, 0.75	7.14, 10.72
Re	G2a	Mono-hull, $s = 0.23$	0.5	2.53, 7.14, 20.2

Mass conservation is enforced using a PISO algorithm, resulting in a Poisson equation for pressure. CFDShip-Iowa allows the computation of ship motions (6DOF) by the use of a dynamic overset-grid approach for local grid refinement and large-amplitude motions. In this case, the code SUGGAR [35] is used to obtain the overset domain connectivity between the set of overlapping grids. The simulations run on HPC cluster Cray XT4 (Jade).

3.2 Domain, boundary condition, grids and simulation conditions

The computational domain includes a background orthogonal grid and a boundary layer curvilinear grid conforming to ship geometry. Some particulars of the computational domain are depicted in Fig. 3. Overall, the grid consists of 3 blocks. The background is a Cartesian block, which is clustered near the free surface to resolve the wave field. Its boundaries are $-0.4 \leq X \leq 3.6$, $0 \leq Y \leq 1.3$ and $-0.7 \leq Z \leq 0.7$, where the coordinates X, Y and Z are non-dimensional with the length between perpendiculars, L_{PP}. For each demi-hull, two body-fitted "O" type grids are generated around the hull geometry. Splash and wave breaking were observed in the experiment; therefore, an unsteady solution of the full ship, which allows asymmetric modes, may be more accurate. However, owing to the computational demand for resolving the current flow, a symmetry boundary condition is applied with respect to $Y = 0$ and only half of the catamaran is simulated. The ship axis is aligned with the x axis with the bow at $X = 0$ and the stern at $X = 1$, as shown in Fig. 1. The free surface at rest lies at $Z = 0$.

The boundary conditions are summarized in Table 2. They are specified for each face of the computational domain, and proper values are set for each flow variable. At Inlet ($X = -0.4$), the free surface level-set function, which is zero on the free surface, is given by $\phi = -z$; pressure is zero-gradient; turbulence is set to free stream values and the velocity field is set to the free stream velocity vector (U,V,W). At Exit ($X = 3.6$), the boundary is assumed far downstream so that stream-wise viscous effects are zero $\left(\frac{\partial^2 U}{\partial n^2} = \frac{\partial^2 V}{\partial n^2} = \frac{\partial^2 W}{\partial n^2} = 0\right)$; other variables are zero-gradient due to domain truncation. Two far-field boundary conditions are used to limit the domain along Y- and Z-axes. Furthermore, $\frac{\partial \phi}{\partial n} = +1$ at $Z = -0.7$ indicates that the surface is in contact with the liquid phase; $\frac{\partial \phi}{\partial n} = -1$ at $Z = +0.7$ indicates the contact between the top background surface and air. Finally, on the ship hull a no-slip boundary condition is imposed, in which the value for ω is suggested by Menter [34] and is strictly related to the use of the blended $\kappa - \varepsilon/\kappa - \omega$ turbulence model.

Table 5 Verification for $s = 0.23$ at $Fr = 0.5$

Param.	Triplet	R	P	U_I % U_G	$U_{SN} = U_G$ % D
C_T	G1, G2, G3	0.71	0.49	0.27	5.66
	G2, G3, G4	1.62	MD		
Sink	G1, G2, G3	0.37	1.43	0.43	1.41
	G2, G3, G4	−0.37	OC	3.91	1.12
Trim	G1, G2, G3	0.73	0.45	0.10	20.57
	G2, G3, G4	0.753	0.33	0.07	45.82

Six grids are used for the current studies: the number of grid points range from 0.8 to 38.1 M. Grids G1, G2, G3 and G4 are generated with refinement ratio $\sqrt{2}$. They are used for quantitative verification and validation study and enable two grid-triplet studies. Grid G2 is also used for interference study, while grid G2a, generated for the study of Reynolds number effects are obtained by reducing the near wall distance in G2. Finally, for improved wave elevation predictions, a Cartesian refinement block between the demi-hull and symmetry plane is added to G1 to form grid G1R. Tables 3, 4 summarize the grids dimensions and the research studies, respectively.

Table 6 Validation for $s = 0.23$ at $Fr = 0.5$ for grid triplets G1, G2, G3

Param.	INSEAN EFD[a]			
	U_D	U_{SN}	U_V	E
C_T	0.21	5.66	5.66	−4.92
C_f				9.05
C_p				−14.76
Sink	1.31	1.41	1.92	0.85
Trim	2.91	20.57	20.78	−1.39

[a] U_D, U_{SN}, U_V and E are % D

4 Results

This section presents the results of the numerical simulations. Verification and validation study is carried out for integral variables (resistance coefficients, sinkage and trim) as well as for local variables (longitudinal wave cuts); the analysis of the flow field, in terms of wave pattern and wave profiles, with focus on demi-hull separation effects, is shown. Finally, the influence of the Reynolds number on interference is investigated.

4.1 Verification and validation for resistance, sinkage and trim

In order to benchmark current URANS capability for a high-speed catamaran, including sinkage and trim, quantitative verification and validation (V&V) is required. Verification and validation follows the approach presented in Stern et al. [36], while for numerical uncertainty, U_{SN}, the factor of safety method proposed by Xing and Stern [37] is adopted. Quantitative V&V is conducted for $s = 0.23$ and $Fr = 0.5$, for resistance (C_T), sinkage and trim.

The verification study is carried out for two grid triplets: (G1, G2, G3) and (G2, G3, G4). The results are summarized in Table 5. R is the convergence ratio, defined as:

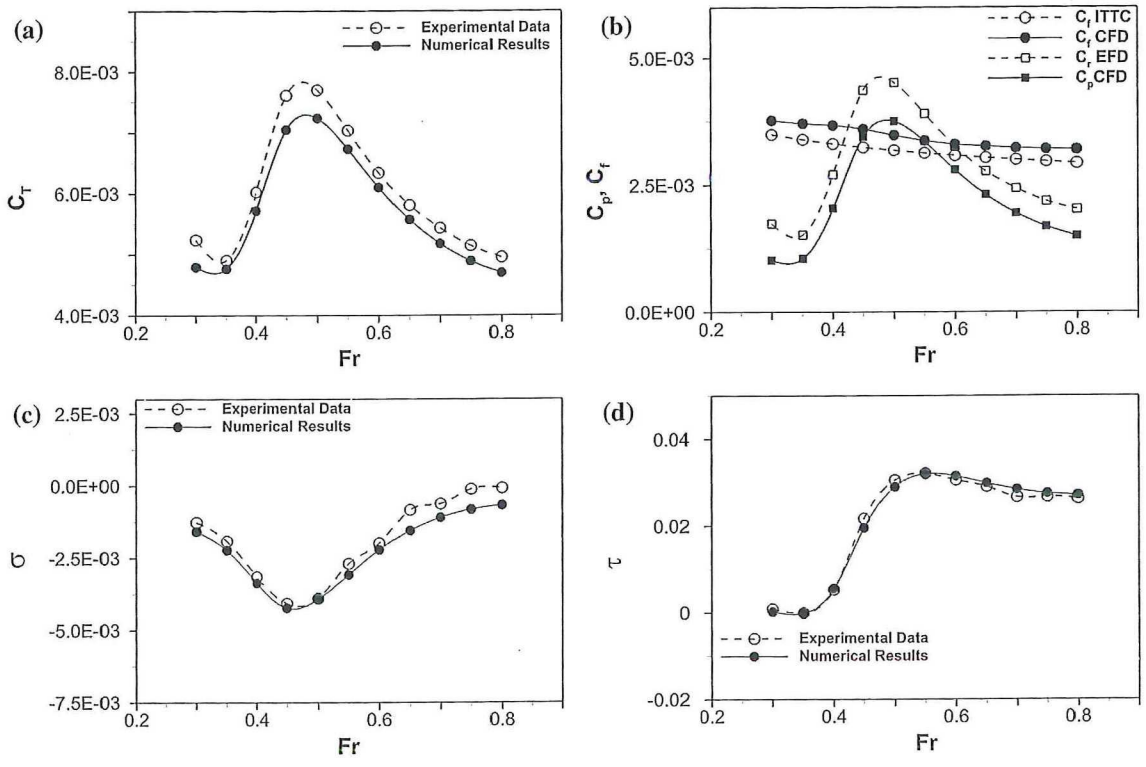

Fig. 4 CFD simulations (Grid G2) for catamaran $s = 0.23$ compared with INSEAN EFD. **a** Total resistance coefficient; **b** pressure and friction coefficients; **c** non-dimensional sinkage; **d** non-dimensional trim

$$R = \frac{S_2 - S_1}{S_3 - S_2} \tag{3}$$

where S_1, S_2 and S_3 are the integral or local numerical solutions corresponding to the fine, medium and coarse grid, respectively. When monotonic convergence is achieved ($0 < R < 1$), the generalized Richardson extrapolation is used for the estimation of numerical error and uncertainty. Consequently, the Richardson extrapolation numerical error can be estimated as:

$$\delta_{RE} = \frac{\varepsilon_{21}}{r^{p_{RE}} - 1} \tag{4}$$

where the order of accuracy, p_{RE}, is given by:

$$p_{RE} = \frac{\ln(\varepsilon_{32}/\varepsilon_{21})}{\ln(r)} \tag{5}$$

$\varepsilon_{32} = S_3 - S_2$, $\varepsilon_{21} = S_2 - S_1$ and r is the grid refinement ratio, which in our case is $\sqrt{2}$. In the factor of safety method, a measure for the distance from the asymptotic range is given by P, which is defined as the ratio between the numerical and the theoretical order of accuracy, $P = p_{RE}/p_{th}$; when solutions are in the asymptotic range, $P \approx 1$ and the actual order of accuracy is close to the theoretical value ($p_{th} = 2$). With this method, the numerical uncertainty, U_{SN}, in the last column of Table 5, is estimated through:

$$U_{SN} = \begin{cases} (2.45 - 0.85P)|\delta_{RE}| & 0 < P \leq 1 \\ (16.4P - 14.8)|\delta_{RE}| & P > 1 \end{cases} \tag{6}$$

The verification studies for C_T, sinkage and trim show that, for each variable, iterative uncertainty, U_I, is acceptably small compared to grid uncertainty, U_G; consequently, the grid quality makes the major contribution to the numerical uncertainty, U_{SN}. Monotonic and oscillatory convergence is achieved for all variables ($0 < R < 1$) in the finer grid triplets (G1, G2, G3); on the contrary, monotonic divergence is observed in the coarser grid triplet (G2, G3, G4). Therefore, the finer grid triplet (G1, G2, G3) is used for validation study. For this case, Table 5 shows that the order of convergence for C_T is close to $P \approx 0.5$, and first-order accuracy is attained; for sinkage, $P \approx 1.5$, which indicates a third order accuracy; finally, for trim a first-order convergence is attained (a value around $P = 0.5$ is found). The numerical uncertainties are very low for resistance coefficient and for sinkage, the highest value estimated is around 20 % for trim angle.

Table 6 summarizes the results of the validation study. The comparison error is computed as:

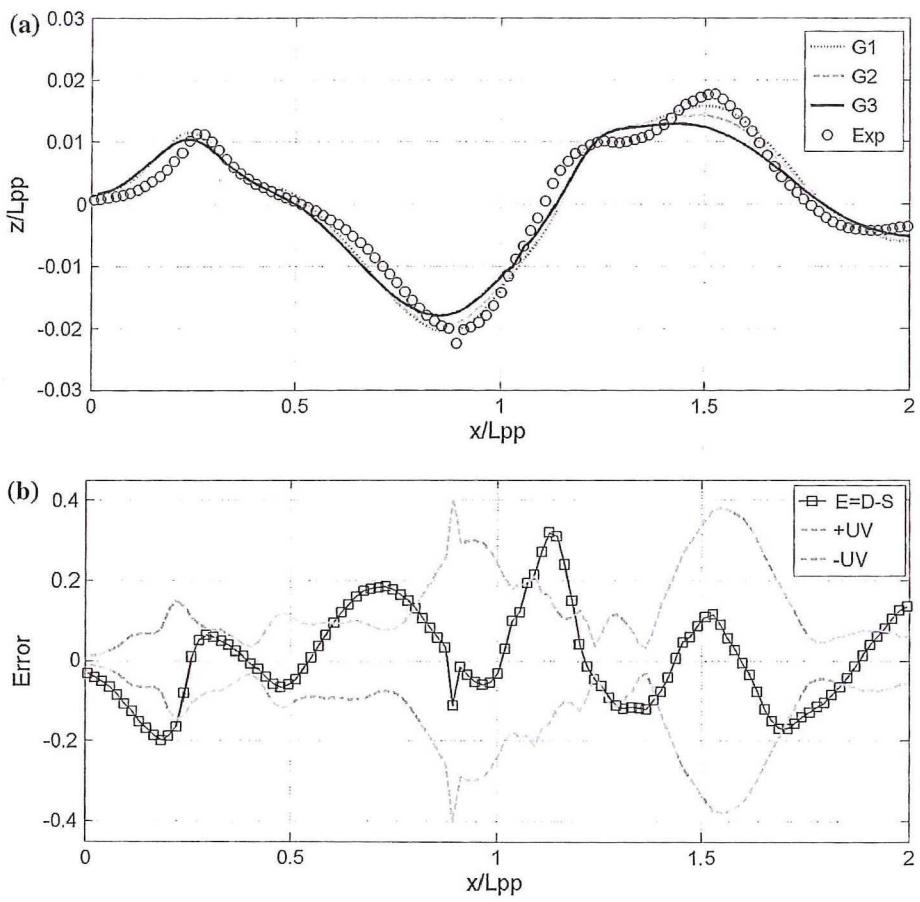

Fig. 5 Grid study and validation of wave profile at Probe 9. The error values are normalized with the maximum height of wave profile ζ_{max}

$$E = \frac{S_1 - D}{D}\% \tag{7}$$

where D is the experimental data; the validation uncertainty, U_V, which takes into account both U_{SN} and experimental uncertainty U_D, is defined as:

$$U_V^2 = U_{SN}^2 + U_D^2 \tag{8}$$

When $|E| < U_V$, the combination of all the errors in D and S is smaller than U_V, and validation is achieved at the U_V interval. The highest error is observed for pressure resistance coefficient and amounts to 14 %. For each variable, the comparison error is lower than the corresponding U_V, indicating thus that validation is achieved at 5, 2 and 20 % D for resistance, sinkage and trim, respectively. The validation level for trim is, however, large and reduction in U_V requires reduction in numerical uncertainty.

Figure 4 shows the comparison between numerical results and experimental data over the whole Fr range, for the catamaran configuration corresponding to $s = 0.23$. Overall, a good agreement between the numerical solution and the experiments is achieved. The average comparison errors over all Fr amount to $E = 5$, 9 and 4.7 % D for C_T, sinkage and trim, respectively, where the highest error computed for sinkage is mainly due to the differences at larger Fr. The differences between C_f and the ITTC model correlation line, and between C_p and C_r equally contribute to the difference between computed and experimental C_T.

4.2 Verification and validation for wave elevation

A further validation test of the numerical results is provided by the comparison of the numerical wave cuts with the measurements obtained by INSEAN. Quantitative V&V is conducted for $s = 0.23$ and $Fr = 0.5$.

The verification and validation procedure for point variables follows the approach presented in Wilson et al. [38]. The convergence ratio, R, and the order of accuracy, p, for point variables, are defined through the separate L2 norms of ε_{21} and ε_{32} according to the following formulations:

$$\langle R \rangle = \|\varepsilon_{21}\|_2 / \|\varepsilon_{32}\|_2 \tag{9}$$

$$\langle p \rangle = \frac{\ln\left(\|\varepsilon_{32}\|_2 / \|\varepsilon_{21}\|_2\right)}{\ln(r_G)} \tag{10}$$

where $\langle\rangle$ and $\|\|_2$are used to denote a profile-averaged quantity and L2 norm, respectively. Numerical errors and

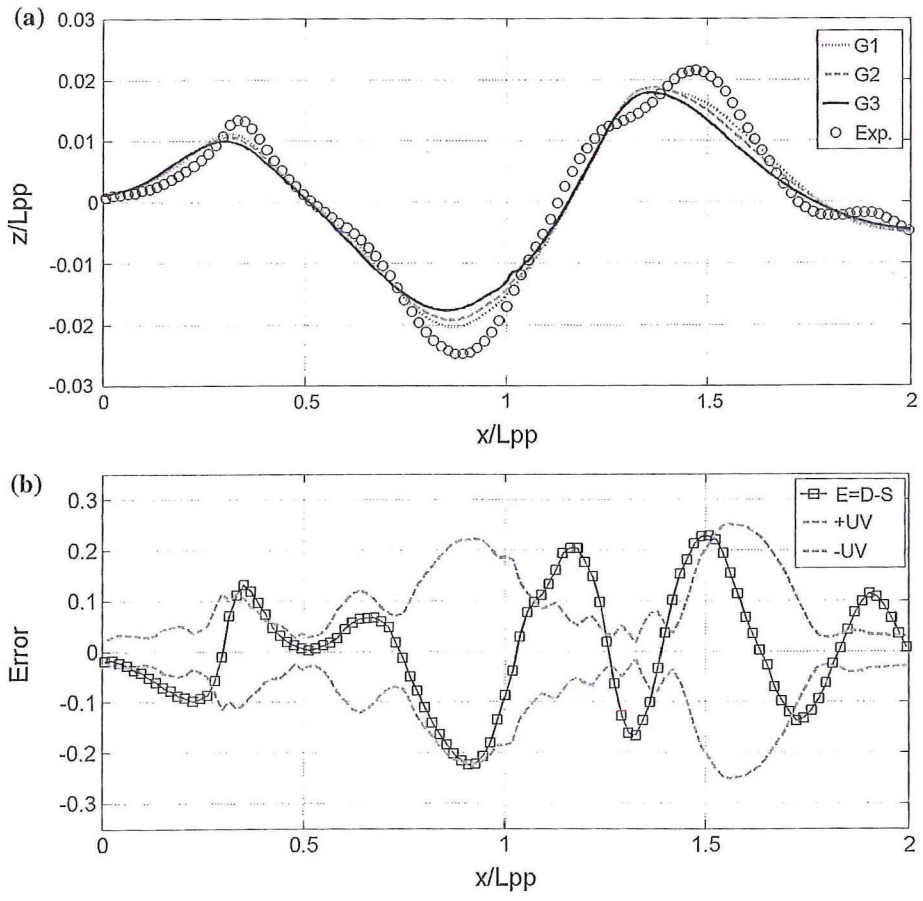

Fig. 6 Grid study and validation of wave profile at Probe 11. The error values are normalized with the maximum height of wave profile ζ_{max}

Table 7 Verification and validation for wave profiles ($s = 0.23$, $Fr = 0.5$)

Location	Verification			Validation		
	R_G	P	U_G	U_D	U_V	E
Probe 9	0.67	0.58	15.01	7.45	16.76	11.56
Probe 11	0.66	0.58	10.74	4.72	11.73	11.58

[a] U_D, U_G, U_V and E are % ζ_{max}

Table 8 CFD simulations with different grids

s	Fr	Grid	$C_T \times 10^3$		Sink		Trim	
			S	ε_{12} % S_1	S	ε_{12} % S_1	S	ε_{12} % S_1
0.23	0.50	G1	7.322	1.17	−11.79	0.27	−1.74	3.71
		G2	7.236	1.66	−11.76	0.73	−1.67	5.24
		G3	7.116		−11.68		−1.58	

ε_{12} % $S_1 = (S_1 - S_2)$ % S_1, where S_1 is the result of finer grid, and S_2 is the coarse grid

grid uncertainties distributions are estimated through Eqs. 4 and 6, respectively, where p_{RE} is given by 10. The L2 norms of these distributions are, then, used to assess verification levels. In order to judge whether validation is globally achieved, the L2 norm of E and U_V distributions, obtained through Eqs. 7 and 8, respectively, is finally evaluated.

Figures 5a and 6a show the longitudinal wave cuts at distances $Y/b = 0.125$ and $Y/b = 0.4166$ from the hull inner side, respectively (Probes 9 and 11). It can be observed that there is a good agreement among numerical and experimental wave profiles. The verification and validation results are summarized in Table 7. The values are normalized with the maximum value of wave profile, ζ_{max}. In both cases, monotonic convergence is achieved; furthermore, results are validated at a level of 16.7 and 11.7 % for Probe 9 and Probe 11, respectively. The V&V procedure shows that, overall, to reduce the validation uncertainty, numerical improvements related to grid quality are needed. Nonetheless, the numerical results can be advantageously used for the analysis of the flow physics involved in the interference phenomena. Distributions of E and U_V as a function of x/L_{PP} are plotted in Figs. 5b and 6b.

4.3 Resistance, sinkage and trim

The results presented in this section are obtained by the use of grid G2, which is the best compromise between grid quality, computational effort and solution accuracy. The

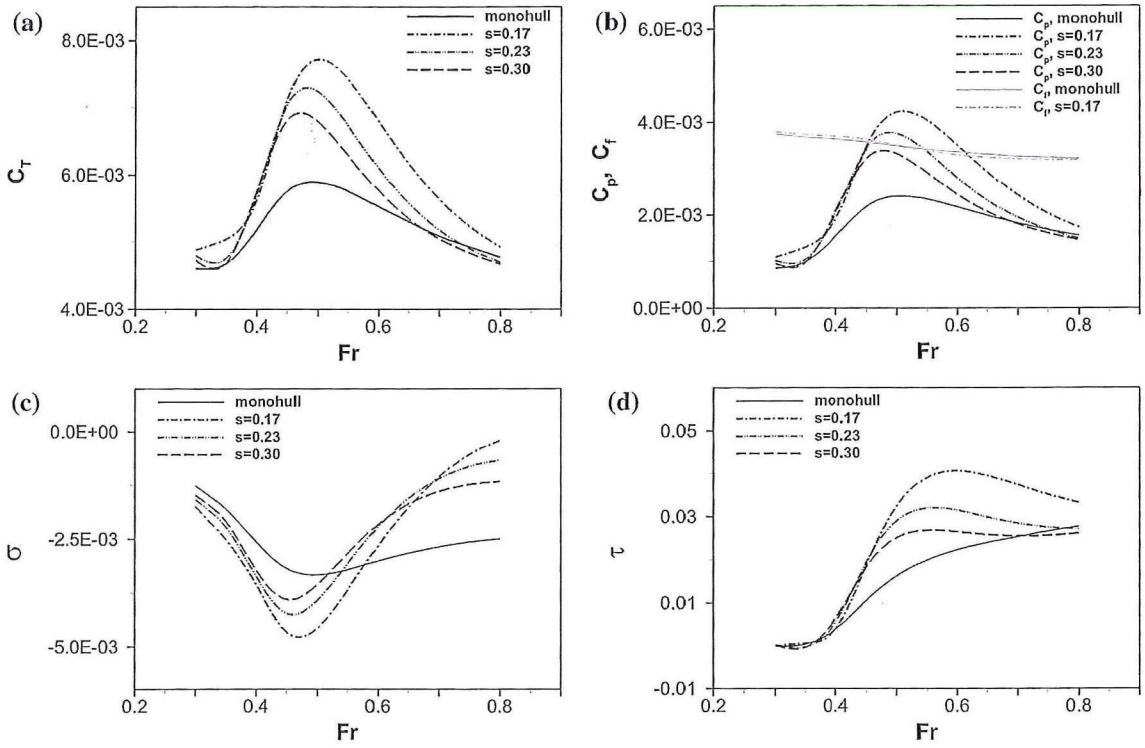

Fig. 7 CFD simulations for mono-hull and catamaran (Grid G2). **a** Total resistance coefficient; **b** pressure and friction resistance coefficients; **c** non-dimensional sinkage; **d** non-dimensional trim

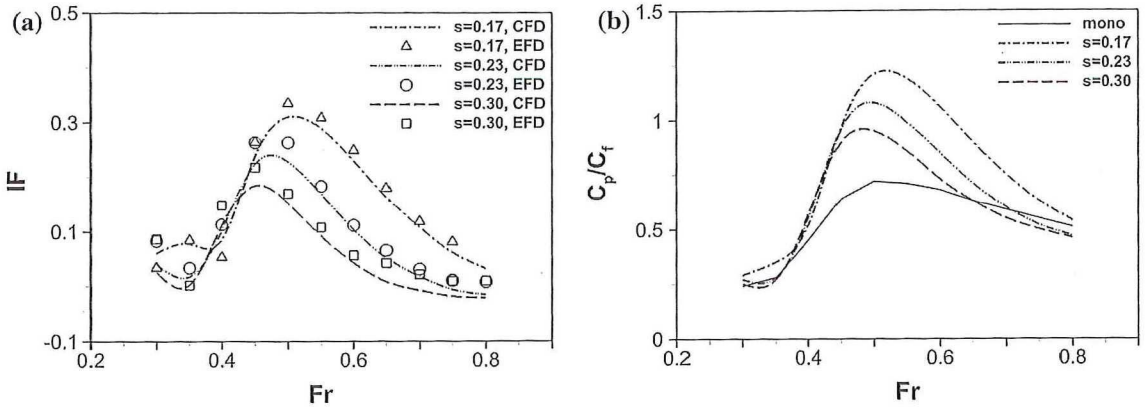

Fig. 8 **a** Interference factor: numerical values compared with INSEAN EFD; **b** numerical C_p/C_f

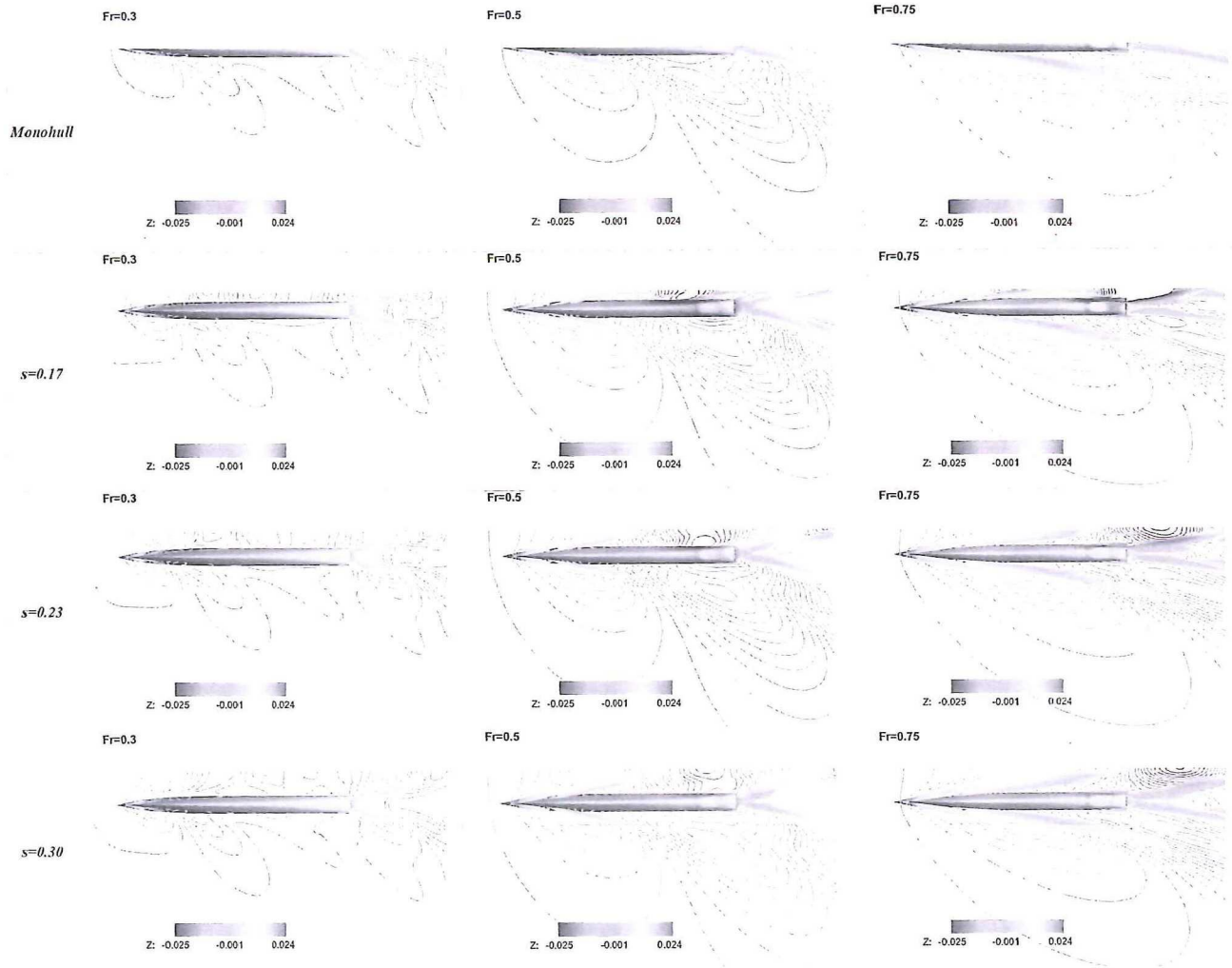

Fig. 9 Wave patterns and surface pressure distribution on the hull surface at three *Fr* for mono-hull and for catamaran at three separation distances

study, summarized in Table 8, shows that the solution changes for the finest grids are less than 1.2 % S_1 for resistance, less than 0.3 % S_1 for sinkage, and less than about 4 % S_1 for trim, owing to the different order of convergence of each variable. In conclusion, even though the solutions are far from the asymptotic range, the

differences between the coarser and the finer grids are relatively small, and justify, therefore, the use of the results obtained with grid G2 for the discussion of the numerical findings.

Numerical results both for the mono-hull and the catamaran, at several separation distances, are plotted in Fig. 7, including C_T, C_p, C_f, sinkage and trim. About the resistance coefficient (Fig. 7a), similarly to EFD data, at low and high speed, i.e., $Fr \leq 0.35$ and $Fr \geq 0.75$, the differences between the mono-hull and the catamaran are small; also, at $Fr \leq 0.45$ and $Fr \geq 0.65$, the hull configuration seems to have little influence on C_T. On the contrary, a clear dependency of C_T on the separation length, s, is observed near the hump ($Fr \approx 0.5$): as the separation distance decreases, the maximum value of C_T increases and occurs at higher Fr values. Figure 7b shows that the augmented resistance experienced by the catamaran is mostly due to an increase in the wave resistance, C_p, and consequently to the interference phenomena between the two hulls. Another hump around $Fr = 0.3$ is found in the experiments, as reported in Fig. 2 [24]. However, the hump is not distinct in CFD simulations. A local minimum is, finally, observed in the experiments at $Fr = 0.35$ (Fig. 2), where C_T decreases as the distance between the hull increases. Negligible or slightly favorable interference is obtained around this point. This local minimum is not predicted in CFD simulations.

Sinkage difference among all the configurations is noticeable in the whole Fr range (Fig. 7c), even for low or high Froude number values, where the resistance difference among the configurations is very small. Sinkage reaches a minimum value for $Fr = 0.5$ in mono-hull, and for $Fr = 0.45$ in catamaran configurations. Sinkage in catamarans is more sensitive to Fr change than mono-hull. Finally, the decrease of separation distance increases the sinkage magnitude.

Trim is negligible up to $Fr = 0.35$ for all the configurations (Fig. 7d). Similarly to Insel et al. [1] and Molland et al. [2] results, trim difference becomes clearer when $Fr \geq 0.4$ and catamarans display significant higher trim than mono-hull. When the separation distance increases, trim angle approaches the mono-hull value. Large difference between mono-hull and catamaran can be seen in the Fr range 0.5–0.7, where trim reaches a maximum. At

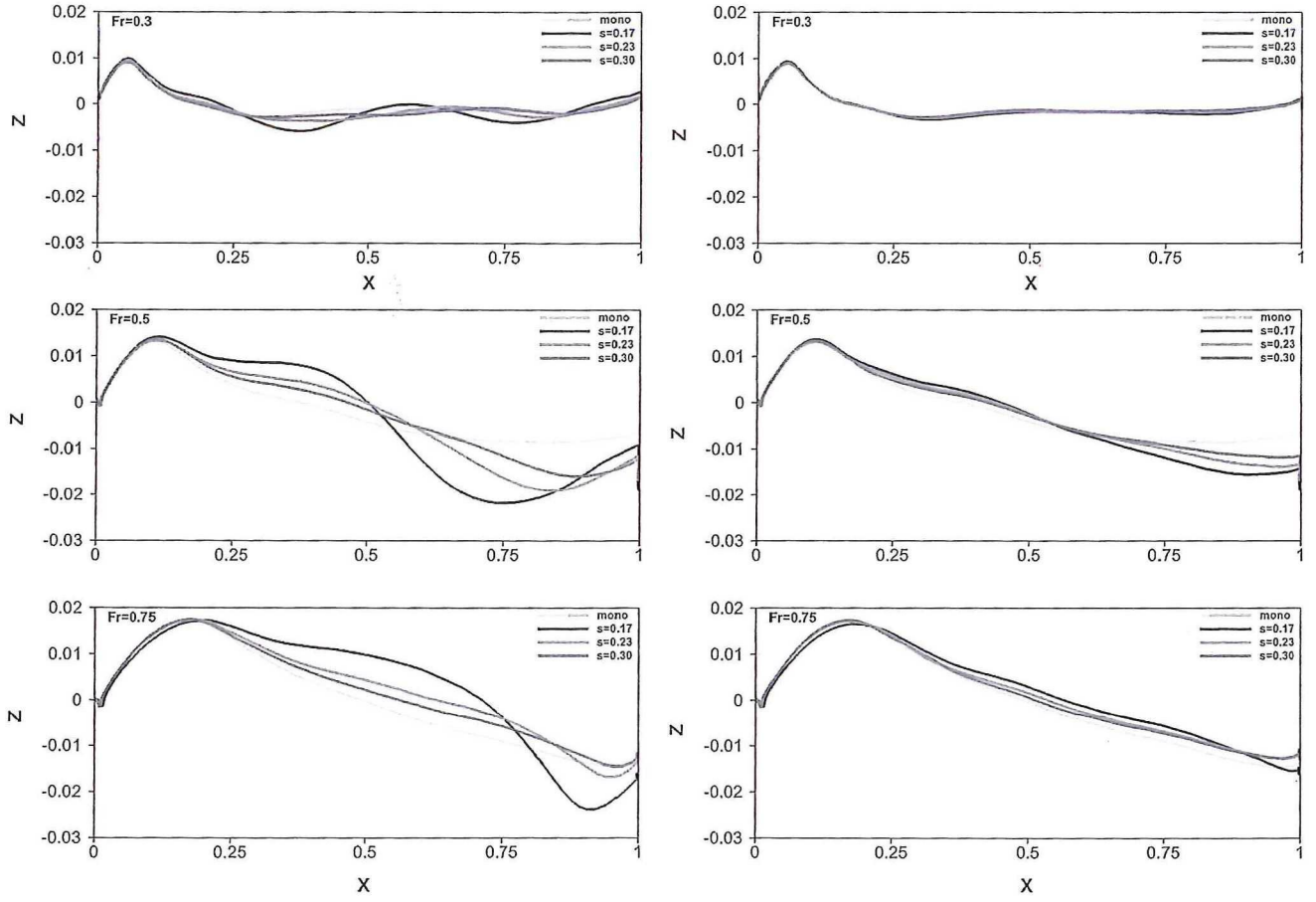

Fig. 10 Numerical wave profiles on the hull surface at three Fr, for mono-hull and catamaran, at three separation distances. Inner side on hull (*left*), outer side on hull (*right*)

higher speed values ($Fr > 0.7$), the effects of demi-hull separation distance on trim are negligible except for the $s = 0.17$ case, which shows a slight difference with respect to the other configurations.

4.4 Interference

Figure 8 shows the comparison between predicted and experimental IF and C_p/C_f values vs. Fr, for all the catamaran configurations. The numerical values used in this section refer to grid G2. The agreement between experiments and computed results is satisfactory. The average errors over the whole speed range amount to 6.4, 6.2 and 8.4 % for $s = 0.17$, 023 and 0.30, respectively.

At low speed (Fig. 8a), i.e., $Fr \leq 0.35$, and at supercritical speed ($Fr \geq 0.75$), the IF value is close to zero. In this case, in fact, the C_T curves (Fig. 7a), for all the s values, collapse on the mono-hull line and the separation distance does not have any influence on catamaran resistance, which is consistent with previous studies [6]. However, differently from Souto-Iglesias et al. [6] and from Broglia et al. [24], in our computations negative IF values are not observed at Fr values near 0.35. As Fr increases, $0.35 < Fr \leq 0.45$, interference becomes large, owing to the larger differences between mono-hull and catamaran C_T values, but with small influence of the separation distance. The interference coefficient reaches a peak around $Fr = 0.5$, similarly to the resistance coefficient behavior, and it is higher for narrower than for wider separation distance. For higher speed ($Fr > 0.5$), IF reduces substantially.

Figure 8b shows C_p/C_f versus Fr. The C_p/C_f ratio directly correlates with the interference factor IF, so that for the Delft catamaran the interference is largely due to the increased pressure component C_p, which increases significantly as the separation distance decreases.

The behavior of resistance, interference factor, sinkage and trim as a function of the Froude number will be related to the flow field and wave patterns obtained by the numerical simulations in the following sections.

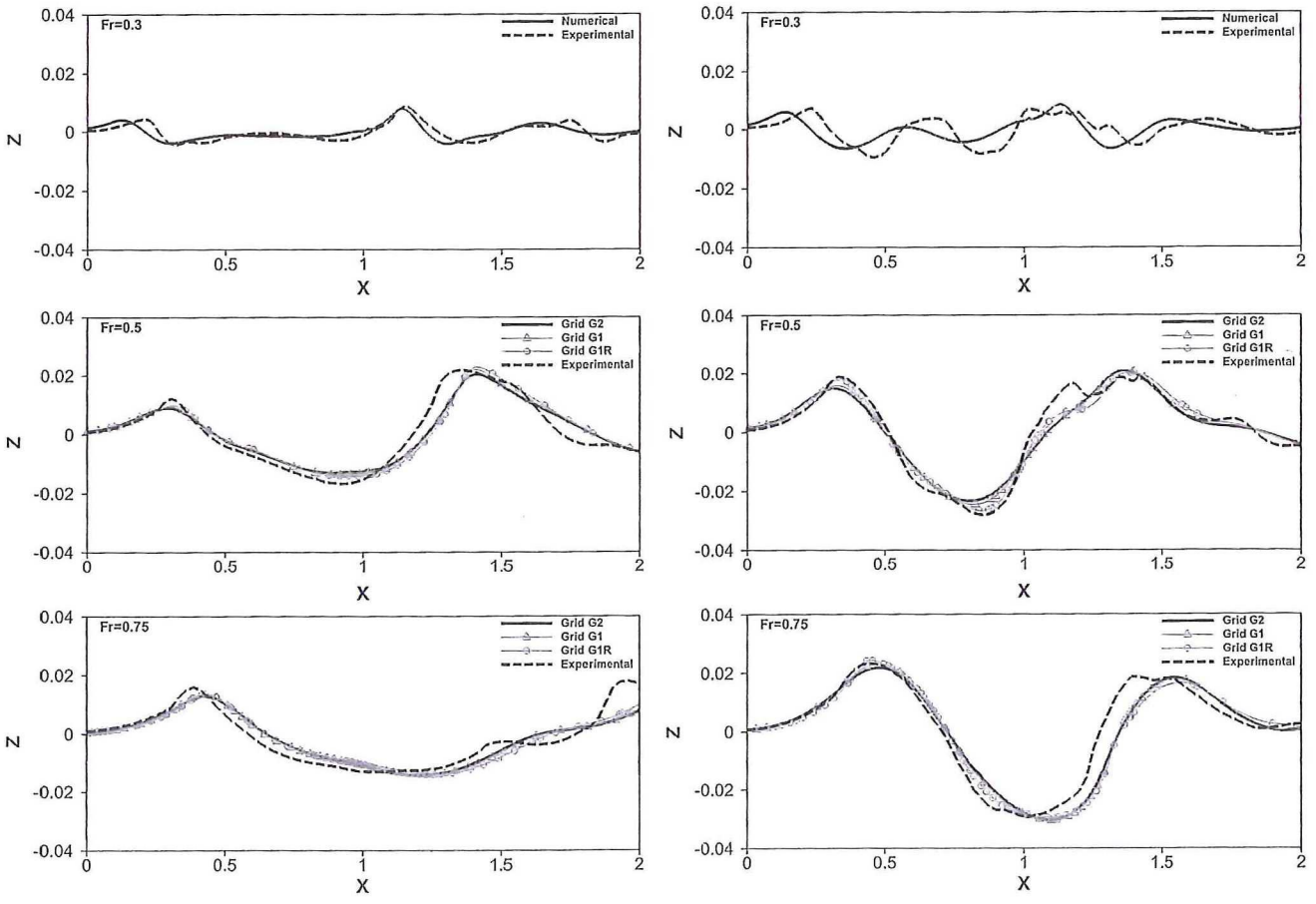

Fig. 11 Longitudinal wave cuts at $Fr = 0.3$, $Fr = 0.5$ and $Fr = 0.75$ for the catamaran configuration $s = 0.17$. Comparison between numerical results obtained using grids G2, G1 and G1R, and INSEAN EFD. Left: Location 3 (*outboard*); right: Location 11 (*inboard*)

4.5 Wave pattern and surface pressure

Figure 9 presents the computed wave pattern and hull surface pressure distribution for the mono-hull and for all the three catamaran configurations, at $Fr = 0.3, 0.5, 0.75$.

Overall, the mono-hull displays a typical Kelvin wave pattern of diverging and transverse waves with crest at the bow. At $Fr = 0.5$, $\lambda/L_{PP} \approx 2$ and the first trough is at the stern; as a consequence, the pressure drag is maximum. The wave patterns for the catamarans are more complex than those for the mono-hull. Strong interference phenomena are observed in the inner region, where the interacting wave systems between the hulls result in larger wave amplitudes (higher wave crests and deeper wave troughs). These are more prominent as the separation distance decreases. On the contrary, the external wave pattern is slightly affected by the presence of the twin hull.

The variation of the resistance coefficient as well as the interference factor as functions of speed and separation distance (Figs. 7, 8) is strictly related to the position and magnitude of the waves crests and troughs which develop in the inner region between demi-hulls. For a fixed separation distance, at low Fr ($Fr = 0.3$), the crests and troughs are relatively small and low C_T values occur; the whole wave pattern is quite similar to the mono-hull and, as the interaction between the waves systems in the inner region is weak, the effects of separation distance on IF are negligible (IF $\approx$ *0*). As Fr increases, ($Fr = 0.5$), the wave trough is deeper and moves downstream closer to the stern; therefore, the resistance reaches its maximum; furthermore, due to the higher amplitude of the interfering waves with respect to the mono-hull, IF increases significantly. At $Fr = 0.75$, the wave trough moves behind the stern and a reduction of C_T occurs; the interaction occurs downstream and a consequent reduction of IF is observed.

In the range of speed values where significant dependency of C_T on the separation length is observed ($Fr \approx 0.5$), as the gap between the hulls increases, the wave trough moves behind the stern, with lower depression; consequently, a reduction of resistance coefficient is obtained. This also implies that, at small separation length, the wave trough reaches the stern at higher speeds than the larger separation gaps, and consequently the C_T peak is shifted to higher Fr.

Sinkage and trim are strongly affected by the pressure distributions on the hull surfaces. From Fig. 9 it is clear

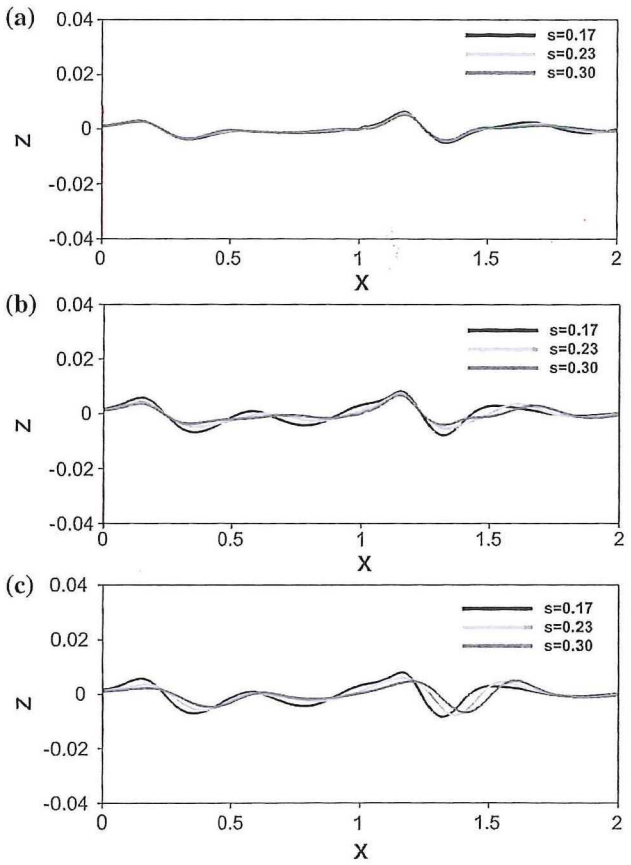

Fig. 12 Numerical longitudinal wave cuts at $Fr = 0.3$. **a** outboard location; **b** inboard location 11; **c** center line

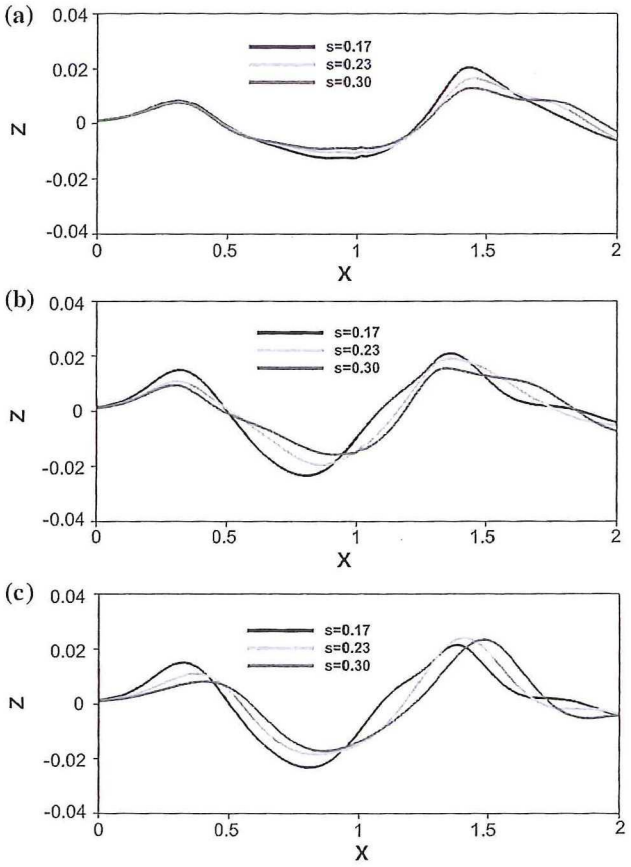

Fig. 13 Numerical longitudinal wave cuts at $Fr = 0.5$. **a** outboard location; **b** inboard location 11; **c** center line

that the wave trough, which arrives at the stern with the highest intensity ($Fr = 0.5$, $s = 0.17$), causes a large depression on hull surface. Under these conditions, sinkage and trim reach their absolute maxima (Fig. 7c and d). Figure 10 shows the wave profile on the hull surface both for mono-hull and catamaran configurations. At $Fr = 0.5$, the wave elevation has a crest at the bow and a trough at the stern; it creates large pressure resistance as well as large sinkage and trim values, which vary with the separation length according to Fig. 7. At low speed, $Fr = 0.3$, the wave height is low and only a small area of the hull surface is affected by the wave trough depression. Finally, at high speed, $Fr = 0.75$, the wavelength is large enough to shift the wave trough downstream of the stern; the inner wave profile on the catamaran hulls is similar to the mono-hull one; therefore, the sinkage and the trim approach the mono-hull values.

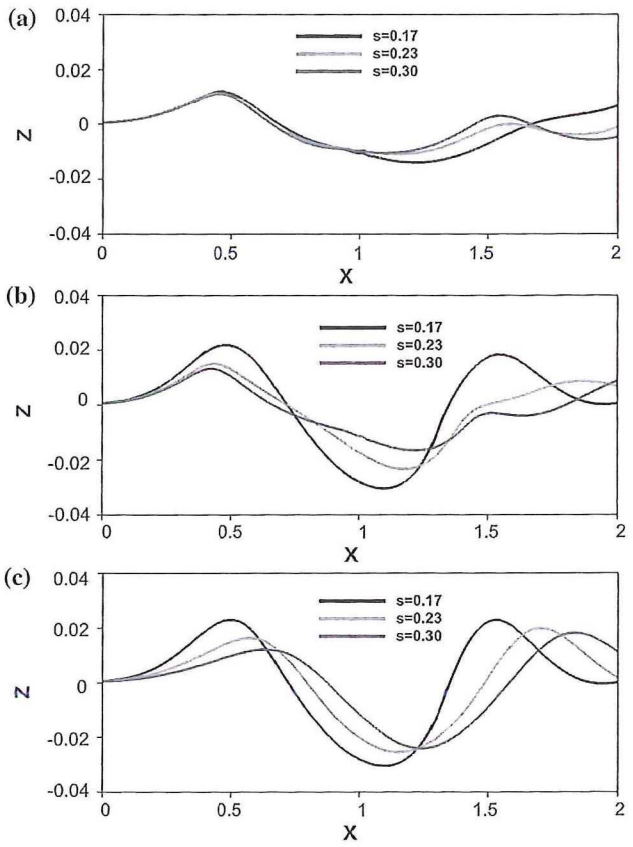

Fig. 14 Numerical longitudinal wave cuts at $Fr = 0.75$. **a** outboard location; **b** inboard location 11; **c** center line

4.6 Longitudinal wave cuts

INSEAN experimental wave cuts were measured at outboard locations (1–4), inboard locations (9–12) and at centerline. Figure 11 shows a comparison between the computational and experimental wave cuts, for the inboard location 11 (on the right) and the outboard location 3 (on the left). In Fig. 11, the wave cuts are obtained for $s = 0.17$ using grids G2, G1 and G1R, to evaluate the effects of grid refinement on wave elevation predictions. This study is carried out for $Fr = 0.5$ and $Fr = 0.75$. Overall, the simulations show fairly good agreement for all the cases. The finer grid G1 improves the wave predictions with respect to G2, and further improvements are obtained with the finest grid G1R. However, the improvements in solution accuracy do not justify the higher computational effort due to the finer grids. In fact, for $Fr = 0.75$, the average error computed using grid G2 amounts to 8.02 %, it reduces to 7.6 % using grid G1; the error amounts to 7.31 % using grid G1R. Similar values are obtained for $Fr = 0.5$.

Figures 12, 13, 14 show the numerical longitudinal waves elevations with varying the separation distance, in the outer side, in the inner side and at the center plane, for several speed values. It can be observed that the external wave cuts are weakly affected by the demi-hull separation distance; in particular, along the hull ($0 < X < 1$) the differences between the wave cuts are negligible, while, owing to the waves interactions at and after the stern, some differences can be observed for $X > 1$. However, the most relevant effects of interference occur in the inner region, where large differences occur between the inner wave profiles, with varying the separation length. The figures put

Table 9 Effects of Reynolds number on resistance, sinkage and trim for catamaran configuration $s = 0.23$ and mono-hull, at $Fr = 0.5$

s	L (m)	$Re(10^6)$	E^a							
			$C_f \times 10^3$	$C_p \times 10^3$	$C_T \times 10^3$	Sinkage (mm)	Trim (deg)	$C_{T,\,cat} - C_{T,\,mono}$	IF_f	IF_p
0.23	1.5	2.53	18.5	0.4	9.5	−0.5	−0.4	**1.0**	−1.7	0.7
	3.0	7.14								
	6.0	20.2	−15.4	0.02	−7.8	0.2	0.5	**−0.35**	3.0	−0.6
Mono	1.5	2.53	19.2	0.1	11.5	0.3	−0.1			
	3.0	7.14								
	6.0	20.2	−15.9	0.23	−9.5	−0.1	0.1			

$E^a = (S - S^a)\ \%\ S^a$, S^a is the result of $L_{PP} = 3.0$ m

in evidence the position and the magnitude of the wave trough and confirm what is already observed: the wave trough becomes deeper and moves downstream with increasing ship speed, while, at fixed Fr, it is deeper with reducing the separation length.

4.7 Study of Reynolds number effects

The effects of Reynolds number (Re) on resistance, sinkage, trim and on the interference factor are studied for $s = 0.23$, $Fr = 0.5$ and $Re = 2.53 \times 10^6$, 7.14×10^6, and 20.2×10^6 corresponding to $L_{PP} = 1.5$, 3 and 6, respectively. Simulations are conducted using grid G2a, in which the near wall distance is reduced with respect to grid G2, so that y^+ ranges from 0.1 to 0.6.

Results are summarized in Table 9 for both $s = 0.23$ and the mono-hull. They show that, overall, the total resistance decreases by about 20 % over the whole Re range, both for $s = 0.23$ and for the mono-hull, mainly owing to the reduction of frictional resistance component, C_f, rather than the pressure component, C_p (it decreases by less than 1 % over the Re range).

A reduction in sinkage and trim is also registered over the whole Re range. Both for $s = 0.23$ and the mono-hull, it amounts to less than 1 % and can then be neglected.

Finally, to evaluate the effects of Re on the interference coefficient, the frictional and pressure IF are computed within the Re range and the results display an increase amounting to 4.7 % for frictional IF and a reduction by 1.3 % for the pressure IF. Overall, the global IF reduces for increasing Re. However, the Re effects are small and can be, therefore, neglected.

5 Conclusions

A numerical study has been presented with focus on the effects of Froude number and of the separation distance of the hulls on the resistance, sinkage and trim of a multi-hull vessel. The aim of this work was to assess the predictive current URANS capability for a high-speed catamaran, including sinkage and trim. Consequently, a verification and validation study was carried out both for global and local variables.

The following conclusions can be drawn:

- Ship motions are predicted with reasonable accuracy for most of the cases under investigation, the maximum average error, over the whole Fr range, amounting to 8.9 % D for sinkage.
- The verification and validation study proves that the major source of errors is due to grid quality. Numerical errors are, however, acceptably small. Overall, the numerical model is validated and the numerical analysis constitutes a useful tool to gain a deep insight into the flow physics involved in the interference phenomena.
- The effects of the Reynolds number, and therefore of viscosity, on interference are small compared to waves interaction and can be therefore neglected.

Acknowledgments This work was supported by Office of Naval Research (ONR), grant of N000141010017, under the administration of Dr. Patrick Purtell. The authors appreciate INSEAN who provides the EFD data for this study.

References

1. Insel M, Molland AF (1992) An investigation into the resistance components of high speed displacement catamarans. Royal Inst Naval Archit 134:1–20
2. Molland AF, Wellicome JF, Couser PR (1996) Resistance experiments on a systematic series of high speed displacement catamarans forms: variation of length-displacement ratio and breadth-draught ratio. Trans Royal Inst Naval Archit 138:59–71
3. Cheng XN, Sharma SD, Stuntz N (2003) Wave reduction by S-catamaran at supercritical speeds. J Ship Res 47:145–154
4. Millward A (1992) The effect of hull separation and restricted water depth on catamaran resistance. Trans Royal Inst Naval Archit 134:341–349
5. Molland A, Wilson P, Taunton D, Chandraprabha S, Ghani P (2004) Resistance and wash measurements on a series of high speed displacement monohull and catamaran forms in shallow water. Int J Marit Eng 146:19–38
6. Souto-Iglesias AR, Zamora-Rodríguez R, Fernández-Gutiérrez D, Pérez-Rojas L (2007) Analysis of the wave system of a catamaran for CFD validation. Exp Fluids 42:321–332
7. Aubault A, Yeung R (2009) Multi-hull interference wave-resistance in finite depth waters. In: Proceedings of the 24th international workshop on water waves and floating bodies, Zelenogorsk
8. Moraes HB, Vasconcellos JM, Latorre RG (2004) Wave resistance for high-speed catamaran. Ocean Eng 31:2253–2282
9. Tarafder MS, Suzuki K (2007) Computation of wave-making resistance of a catamaran in deep water using a potential-based panel method. Ocean Eng 34:1892–1900
10. Yeung RW, Wan H (2008) Multihull and surface-effect ship configuration design: a framework for powering minimization. J Offshore Mech Arct Eng 130:1–9
11. Bruzzone D, Ferrando M (1995) Numerical evaluation of the steady free surface flow for catamaran hull forms. In: Proceedings of the III symposium on high speed marine vehicles, Naples, April 1995, pp 187–198
12. Stern F, Carrica P, Kandasamy M, Gorski J, ODea J, Hughes M, Miller R, Hendrix D, Kring D, Milewski W, Hoffman R, Cary C (2006a) Computational hydrodynamic tools for high-speed transports. Trans SNAME, Vol. 114
13. Stern F, Carrica PM, Kandasamy M et al. (2008) Computational hydrodynamic tools for high-speed sealift: phase II final report. IIHR Technical Report No. 465
14. Kandasamy M, Peri D, Ooi SK, Carrica P, Stern F, Campana EF, Osborne F, Cote J, Macdonald N, Waal ND (2011) Multi-fidelity optimization of a high-speed foil-assisted semi-planing catamaran for low wake. J Mar Sci Technol 16:143–156
15. Milanov E, Zlatev Z (2011) Experimental and computational studies of high-speed catamaran calm water maneuvering. RTO/AVT-161 Final Report, Chapter 24

16. Van't Veer R (1998a) Experimental results of motions, hydrodynamic coefficients and wave loads on the 372 catamaran model. TU Delft Report, No.1129
17. Van'tVeer R (1998b) Experimental results of motions and structural loads on the 372 catamaran model in head and oblique waves. TU Delft Report, N.1130
18. Bouscasse B, Broglia R, Stern F (2013) Experimental investigation of a fast catamaran in head waves. Ocean Eng 72:318–330
19. Broglia R, Bouscasse B, Jacob B, Zaghi S, Olivieri A, Stern F (2011a) Calm water and seakeeping investigation for a fast catamaran. In: Proceedings of the 11th international conference on fast sea transportation (FAST2011), Honolulu
20. Broglia R, Zaghi S, Mascio AD (2011b) Numerical simulation of interference effects for a high-speed catamaran. J Mar Sci Technol 16:254–269
21. Broglia R, Aloisio G, Falchi M, Grizzi S, Zaghi S, Felli M, Miozzi M, Pereira F, Di Felice F, Stern F (2012) Measurements of the velocity field around the DELFT 372 catamaran in steady drift. In: Proceedings of the 29th symposium on naval hydrodynamics, Gothenburg
22. Castiglione T, Stern F, Kandasamy M, Bova S (2011) Numerical investigation of the seakeeping behavior of a catamaran advancing in regular head waves. Ocean Eng 38:1806–1822
23. Zaghi S, Broglia R, Di Mascio A (2011) Analysis of the interference effects for high-speed catamarans by model tests and numerical simulations. Ocean Eng 38(17–18):2110–2122
24. Broglia R, Jacob B, Zaghi S, Stern F, Olivieri A (2014) Experimental investigation of interference effects for high-speed catamaran. Ocean Eng 76:75–85
25. Castiglione T, He W, Stern F, Bova S (2013) URANS simulation of catamaran interference in shallow water. J Mar Sci Technol. doi:10.1007/s00773-013-0230-5
26. Visonneau M, Deng GB, Queutey P, Wakers J, Mallol B (2012) Anisotropic grid adaption for RANS simulation of a fast manoeuvring catamaran. In: 4th high performance yacht design conference, Auckland, pp 172–180
27. Kandasamy M, He W, Takai T, Tahara Y, Peri D, Campana E, Wilson W, Stern F (2011b) Optimization of waterjet propelled high speed ships – JHSS and Delft catamaran. In: Proceedings of the 11th international conference on fast sea transportation (FAST2011), Honolulu
28. Chen X, Diez M, Kandasamy M, Campana EF, Stern F (2013) Design optimization of the waterjet-propelled DELFT catamaran in calm water using URANS, design of experiments, metamodels and swarm intelligence. In: Proceedings of the 12th international conference on fast sea transportation (FAST2013), Amsterdam
29. Diez M, He W, Campana E, Stern F (2013a) Uncertainty quantification of DELFT catamaran resistance, sinkage and trim for variable Froude number and geometry using metamodels, quadrature and Karhunen-Loeve expansion. J Mar Sci Technol (in press)
30. Diez M, Chen X, Campana EF, Stern F (2013b) Reliability-based robust design optimization for ships in real ocean environment. In: Proceedings of the 12th international conference on fast sea transportation (FAST2013), Amsterdam
31. Zlatev Z, Milanov E, Chotukova V, Sakamoto N, Stern F (2009) Combined model-scale EFD-CFD investigation of the maneuvering characteristics of a high speed catamaran. In: 10th international conference on fast sea transportation FAST 2009, Athens
32. Carrica P, Hosseini H, Stern F (2012) CFD analysis of broaching for a model surface combatant with explicit simulation of moving rudders and rotating propellers. Comput Fluids 53:117–132
33. Carrica P, Wilson RV, Noack RW, Stern F (2007) Ship motions using single-phase level set with dynamic overset grids. Comput Fluids 36:1415–1433
34. Menter FR (1994) Two-equation eddy viscosity turbulence models for engineering applications. AIAA J 32:1598–1605
35. Noack R (2005) SUGGAR: a general capability for moving body overset grid assembly. In: AIAA paper 2005-5117, 17th AIAA computational fluid dynamics conference, Ontario
36. Stern F, Wilson R, Shao J (2006) Quantitative approach to V&V of CFD simulations and certification of CFD Codes. Int J Numer Methods Fluids 50:1335–1355
37. Xing T, Stern F (2010) Factors of safety for Richardson extrapolation. J Fluids Eng 132:1–13
38. Wilson R, Stern F, Coleman HW, Paterson EG (2001) comprehensive approach to verification and validation of cfd simulations- part 2: application for RANS simulation of a cargo/container ship. J Fluids Eng 123:803–810